J Neurophysiol 108: 479–490, 2012.
First published April 18, 2012; doi:10.1152/jn.00004.2012.

Detection of tactile inputs in the rat vibrissa pathway

Douglas R. Ollerenshaw, Bilal A. Bari, Daniel C. Millard, Lauren E. Orr, Qi Wang, and Garrett B. Stanley

Coulter Department of Biomedical Engineering, Georgia Institute of Technology and Emory University, Atlanta, Georgia

Submitted 4 January 2012; accepted in final form 15 April 2012

Ollerenshaw DR, Bari BA, Millard DC, Orr LE, Wang Q, Stanley GB. Detection of tactile inputs in the rat vibrissa pathway. *J Neurophysiol* 108: 479–490, 2012. First published April 18, 2012; doi:10.1152/jn.00004.2012.—The rapid detection of sensory inputs is crucial for survival. Sensory detection explicitly requires the integration of incoming sensory information and the ability to distinguish between relevant information and ongoing neural activity. In this study, head-fixed rats were trained to detect the presence of a brief deflection of their whiskers resulting from a focused puff of air. The animals showed a monotonic increase in response probability and a decrease in reaction time with increased stimulus strength. High-speed video analysis of whisker motion revealed that animals were more likely to detect the stimulus during periods of reduced self-induced motion of the whiskers, thereby allowing the stimulus-induced whisker motion to exceed the ongoing noise. In parallel, we used voltage-sensitive dye (VSD) imaging of barrel cortex in anesthetized rats receiving the same stimulus set as those in the behavioral portion of this study to assess candidate codes that make use of the full spatiotemporal representation and to compare variability in the trial-by-trial nature of the cortical response and the corresponding variability in the behavioral response. By application of an accumulating evidence framework to the population cortical activity measured in separate animals, a strong correspondence was made between the behavioral output and the neural signaling, in terms of both the response probabilities and the reaction times. Taken together, the results here provide evidence for detection performance that is strongly reliant on the relative strength of signal versus noise, with strong correspondence between behavior and parallel electrophysiological findings.

psychometric performance; ideal observer; voltage-sensitive dye

HOW THE BRAIN INTEGRATES sensory information, and how it ultimately uses that information to initiate a motor response, are among the most important questions facing the field of sensory neuroscience. Given that most rodents are nocturnal and rely heavily on their facial whiskers for navigation and survival, the rodent vibrissa system has evolved into an incredibly sophisticated sensorimotor system (Diamond et al. 2008; Petersen 2007). Recent studies have shown that the vibrissa system is capable of a wide range of sensory tasks, such as whisker contact detection (Stüttgen et al. 2006; Stüttgen and Schwarz 2008), object localization (Hutson and Masterton 1986; Mehta et al. 2007; O'Connor et al. 2010a, 2010b; Shuler et al. 2002), texture, pattern, and vibrotactile discrimination (Adibi and Arabzadeh 2011; Adibi et al. 2012; Brecht et al. 1997; Carvell and Simons 1990; Gerdjikov et al. 2010; Guic-Robles et al. 1989; Ritt et al. 2008; Von Heimendahl et al. 2007; Wolfe et al. 2008), and aperture width discrimination (Krupa et al. 2001, 2004), but how this information is extracted by the neural circuitry is still largely unknown.

Address for reprint requests and other correspondence: G. B. Stanley, Coulter Dept. of Biomedical Engineering, Georgia Inst. of Technology and Emory Univ., 313 Ferst Dr., Atlanta, GA 30332 (e-mail: garrett.stanley@bme.gatech.edu).

Between the arrival of a stimulus-induced neural signal in the primary sensory cortex and the subsequent motor response, the brain must evaluate the available evidence to determine whether the activity constitutes an important event or is instead environmental or internal noise (Gold and Shadlen 2007). Although the decision process is likely mediated in brain regions that are not purely sensory in nature, by assuming the role of an ideal observer of cortical activation we can learn much about what information is available to downstream structures and evaluate possible candidate codes upon which the computation might actually be based (Jacobs et al. 2009; Wang et al. 2010). Although behavioral outcomes are ultimately linked to the concerted suprathreshold neuronal activity, much of what we currently understand is limited to measurements of single neurons or small groups of neurons, upon which neurometric comparisons to psychometric performance are made (Britten et al. 1992; Shadlen and Newsome 2001; Stüttgen and Schwarz 2008).

In their natural environments, rats and other rodents actively move their whiskers to palpate their surroundings (Berg and Kleinfeld 2003; Bermejo et al. 2002; Brecht et al. 1997; Carvell and Simons 1990; Gustafson and Felbain-Keramidas 1977). The resulting sensory input to this pathway is a complex combination of both the macro- and micromotions of the whisker that relate to the properties of the objects being palpated (Birdwell et al. 2007; Hartmann et al. 2003; Knutsen et al. 2005; Neimark et al. 2003; Ritt et al. 2008; Wolfe et al. 2008) and the self-induced movement of the whisker (Curtis and Kleinfeld 2009; Jenks et al. 2010). Tactile sensing thus explicitly requires the disassociation of self-induced motion from the exogenous sensory input. It has been shown that the pathway encodes information directly related to whisker motion, even when the whiskers are not in contact with an object (Khatri et al. 2009; Leiser and Moxon 2007; Yu et al. 2006). How this might affect the animal's ability to detect an exogenous stimulus in the presence of endogenous, self-generated "noise" has not been well studied.

In this study, head-fixed rats were trained to detect the presence of a brief deflection of their whiskers resulting from a focused puff of air. The animals showed a monotonic increase in response probability and a subsequent decrease in reaction time with increased stimulus strength. High-speed video analysis of whisker motion was used to measure both stimulus-induced as well as self-generated motion of the vibrissae, with evidence indicating that animals were more likely to detect the stimulus during periods of reduced self-motion of the whiskers, thereby allowing the stimulus-induced whisker motion to exceed the ongoing noise. In parallel to the behavioral detection experiments conducted here, we used voltage-sensitive dye (VSD) imaging of barrel cortex in anesthetized rats

receiving the same stimulus set as those in the behavioral portion of this study to assess candidate codes that make use of the full spatiotemporal representation and to compare variability in the trial-by-trial nature of the cortical response (Petersen et al. 2003b) and the corresponding variability in the behavioral response. By application of an accumulating evidence framework to the population cortical activity measured in separate animals, a strong correspondence was made between the behavioral output and the neural signaling, in terms of both the response probabilities and the reaction times.

METHODS

Five Long-Evans rats (Charles River Laboratories, Wilmington, MA; 7 wk of age, ~250 g at beginning of study) were used in the behavioral portion of this study, and two Sprague-Dawley rats (Charles River Laboratories; 200–350 g) were used in the acute VSD experiments. Animals were housed on a 12:12-h light-dark cycle, with all experimental sessions occurring during the light phase. All procedures were in accordance with protocols approved by the Georgia Institute of Technology Animal Care and Use Committee.

Procedure to implant head post. All animals used in the behavioral task were habituated to human contact for a minimum of 5 days prior to the surgical procedure to implant the head post. The head post consisted of a stainless steel machine screw implanted with the threaded end facing upward. All surgical procedures adhered to aseptic principles. Anesthesia was induced with isoflurane at 4–5% in the home cage and was subsequently maintained at 1.5–3% with a nose cone. The depth of anesthesia was monitored through toe-pinch reflexes and a noninvasive continuous measurement of heart rate and blood oxygenation. The scalp was shaved and cleaned of hair with depilatory cream. Animals were then placed in a stereotactic device using nonpenetrating ear bars, and the eyes were covered in ophthalmic ointment to prevent drying. Atropine (0.05 mg/kg sc) and saline (10 ml/kg sc) were administered. The body temperature was thermostatically maintained at 37°C throughout the procedure. The scalp was cleaned with alcohol and a 10% povidone-iodine solution, followed by an injection of lidocaine prior to incision. After the skull was cleared of connective tissue, six to eight holes were drilled and 1.4-mm-diameter stainless steel screws were inserted to anchor the head post to the bone. The head post was then held over the midline, and dental cement was applied over the base of the post and the skull screws. The wound was treated with antibiotic ointment and closed with metal wound clips. Buprenorphine (Buprenex, 0.03 mg/kg sc) was provided as an analgesic, and antibiotics (Baytril, 5 mg/kg im) were administered for a minimum of 3 days postoperatively. Animals were given a minimum of 10 days of recovery before commencing behavioral training.

Water restriction schedule. Water restriction was implemented after a minimum of 10 days of recovery from head post implantation. Training and data recording sessions took place daily, Monday through Friday, and animals did not have access to water in their home cages on those days. Correct responses in the behavioral task were rewarded with 75- to 100-μl aliquots of water, and animals were allowed to continue performing the task until sated. The weight of the animal was tracked daily, and, when necessary, water supplements were provided after the daily experimental session in order to maintain the weight of the animal within 90% of its age-adjusted value. Water was provided ad libitum from Friday afternoon through Sunday afternoon of every week, and for 1 full week every 2 months.

Behavioral apparatus. The behavioral apparatus is illustrated in Fig. 1*A* and was contained in a standard operant conditioning chamber (model 80003, Lafayette Instruments, Lafayette, IN) placed inside a sound- and light-attenuating cubicle (ENV-014, Med Associates, St. Albans, VT). A 6-cm aluminum extension was attached to the animals' head post prior to each behavioral session with a set screw. This head post extension was then held rigidly with a stainless steel clamp extending from the side of the operant conditioning chamber. The body of the animal was contained in a custom-built body restraint box designed to prevent excessive movement while the animal was head fixed. A movable plate at the front of the restraint box provided a location for the animal to rest its forepaws while it was head fixed. The body restraint box was rigidly attached to the floor of the operant conditioning chamber. A stainless steel water spout was directly in front of the animal and served both to deliver water rewards and to measure licking responses. As described by Hayar et al. (2006), the positive lead of an A/D converter was attached to the stainless steel spout and the negative lead was attached to the aluminum floor of the body restraint box. Contact of the animal's tongue with the water spout resulted in an ~600-mV potential change across the two leads. This potential was converted to a binary value, time-stamped, and stored in the data file, thus allowing the onset and offset of each lick of the water spout to be recorded. Water was fed through the spout by a peristaltic pump (model 80204M, Lafayette Instruments). A tone generator (model 80223M, Lafayette Instruments) and a stimulus light (model 80221M, Lafayette Instruments) were installed directly above the water spout. A white noise masking stimulus was delivered through speakers installed in front of the animal, one to either side.

Stimuli consisted of brief 150-ms puffs of air delivered to the vibrissa array on one side of the face (Ahissar et al. 2000; Derdikman et al. 2003; Sosnik et al. 2001). The air puffs were delivered through a custom-built air nozzle constructed from stainless steel hypodermic tubing (19 gauge, 0.032-in. ID at tip; Smallparts). The air puff nozzle was aligned 15° from the longitudinal axis of the animal and aimed such that the air stream impacted the vibrissae approximately halfway between the follicle and the tip, but away from the face. The pressure of the air puff was adjusted with a computer-controlled voltage regulator (part no. QPV1TFEE015CXL, Proportion Air, McCordsville, IN) and varied from 0 to 15 psi. The duration of the air puff was controlled by a miniature normally closed solenoid valve (part no. 5001T332, McMaster-Carr, Atlanta, GA). Both the solenoid and the pressure regulator were placed outside the sound-attenuating chamber to prevent auditory confounds. A second air puff nozzle with identical dimensions was placed adjacent to the stimulus nozzle but aimed such that it did not result in deflections of the whiskers. This second nozzle, referred to as the "distracter nozzle," was programmed to release a puff of air intermittently on a 0- to 5-s uniform distribution and was designed to prevent the animal from cueing off of the sound of the air puff during the behavioral task.

Control of the behavioral task and data logging were performed with custom software written in Microsoft Visual Basic 6. The interior of the behavioral chamber was illuminated with infrared light (model VQ2121, Lorex Technology, Markham ON, Canada), and the animal's behavioral state during the task performance was monitored with a low-speed CCD camera (model DMK 21BF04, The Imaging Source, Charlotte, NC).

Training and behavioral task. After the animal was placed on a water restriction schedule, it was systematically habituated to head fixation and trained to perform the full detection task. The first step was to train the animal to lick the response spout in order to receive a water reward. In this stage of training, the animal was allowed to freely roam the operant conditioning chamber and approach the water spout at will. Water was dispensed on a 1-s interval as long as the animal continued to lick the spout, and the animal was allowed to drink until sated. The animals quickly learned to voluntarily enter the body restraint box to approach the water spout. After 2–3 days, a rubber version of the head post extension was clamped onto the head post and held by hand while the animal drank from the water spout. After the animal was able to tolerate manual fixation without signs of distress, the rubber head post extension was affixed in the head post clamp, allowing a limited degree of mobility. The length of time that

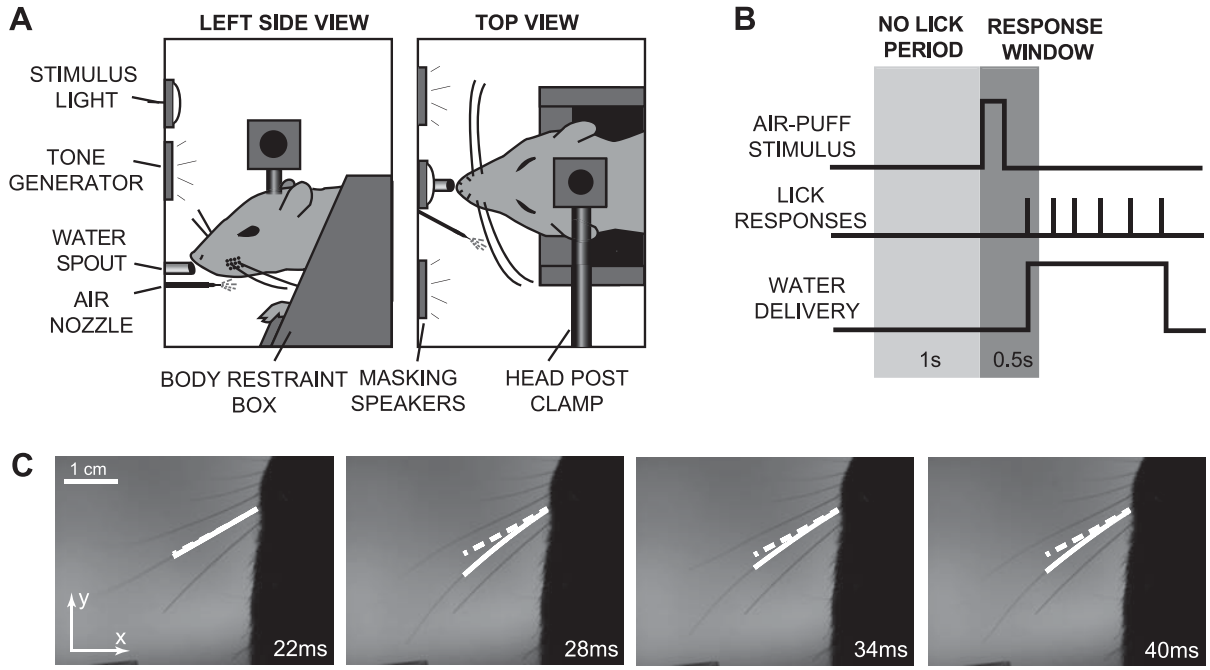

Fig. 1. A go/no-go behavioral detection task was used to probe the sensitivity of head-fixed rats to brief whisker deflections. *A*: schematic of the behavioral apparatus. Head-fixed animals were trained to respond to air puff stimuli delivered to their whiskers by licking a response spout. *B*: timeline of the behavioral task. After a tone, the tactile stimulus was presented at a random time, where the duration between the tone and the stimulus was drawn from a uniform distribution on 1.5–5.5 ms. To discourage guessing, a "no-lick period" was imposed in which any licks within 1 s prior to the forthcoming stimulus resulted in an additional delay of the stimulus. Animals had a 500-ms window in which to respond by licking the spout after the delivery of a stimulus. Responses to air puff (S+) trials were rewarded with a 70- to 100-μl drop of water. Catch (S−) trials were interleaved on 10% of trials, where a distracter nozzle (positioned near the air nozzle but not aimed at the vibrissae) was activated to test for chance response probability. Responses on S− trials were penalized with a 5- to 10-s time-out in which the stimulus light was activated. Failure to respond on S+ trials was not penalized, and correctly withholding on S− trials was not rewarded. *C*: to quantify the strength of the air puff stimulus, high-speed video was recorded while the stimulus was delivered to an anesthetized animal with only a single row of whiskers remaining. Shown are 4 frames from a representative video with a tracking polynomial overlaid on the C2 whisker, which was the whisker that was deflected maximally by the air puff. Although multiple whiskers were deflected, only the maximally deflected whisker was considered for tracking purposes. The polynomial fit to the whisker is designated by the solid white line, while the dashed white line indicates the initial position of the whisker. The coordinate system used in the tracking algorithm is shown in the 1st frame.

the animal was affixed in the head clamp was gradually increased, as was the delay between water rewards.

After the animal was capable of tolerating head fixation for a minimum of 5 min, with a 4-s delay between water rewards, the rubber head post extension was replaced with the aluminum version and the animal was moved to the next stage of training, in which lick responses were conditioned on the air puff stimulus. In this stage of training, the animal was placed on a modified version of the task in which premature licks were not penalized. Thus the animal was able to lick the spout freely, but only the first lick within a maximum of 2 s following a 15 psi puff of air to the whiskers was rewarded with a water drop. The window of opportunity following the air puff was gradually decreased to 500 ms over a number of days. Simultaneously, a delay was added if any licks were detected within a 1-s window preceding the scheduled stimulus delivery time. This delay was gradually increased to 1.5–5.5 s randomly chosen on a uniform distribution. The animals quickly learned to withhold licking until the stimulus was detected. Finally, the white noise masking stimulus and the distracter puffs were added. Training and habituation procedures were based on those described by Schwarz et al. (2010).

In the full version of the task, described schematically in Fig. 1*B*, a 500-ms tone signaled the start of a new trial. The white noise masking stimulus was muted during presentation of the tone. On S+ trials, or those in which the animal was expected to respond, the stimulus delay was drawn from a 1.5- to 5.5-s uniform distribution. To prevent random licking, any licks occurring within 1 s of the scheduled stimulus resulted in a further 1.5- to 5.5-s delay. A trial was categorized as a "hit" if the animal licked the water spout within 500 ms of the air puff stimulus and a "miss" otherwise. Hits were rewarded with a 70- to 100-μl aliquot of water (activation of the peristaltic pump for 1–1.5 s), and misses were not penalized. On each trial, 1 of 11 possible stimulus strengths was randomly chosen (0 psi, 0.375 psi, 0.75 psi, 1.125 psi, 1.5 psi, 1.875 psi, 2.25 psi, 3 psi, 4.5 psi, 7.5 psi, 11.25 psi). The resulting angular deflection velocities of the whiskers were measured by high-speed video analysis of an anesthetized animal undergoing the same range of stimulus strengths (see below). On every fifth trial, a test stimulus consisting of the maximum air pressure (15 psi) was presented to probe the attentional/motivational state of the animal. The test stimulus was repeated if the animal failed to respond, and the session was halted if the animal failed to respond to three consecutive test pulses. Catch trials (labeled S−) were interleaved on 10–20% of trials. S− trials were identical to S+ trials with the exception that only the distracter air puff nozzle was activated at the scheduled stimulus delivery time, thus probing the animal's probability of responding by chance or as a result of potential auditory confounds. Responses on S− trials were labeled as "false alarms" and were penalized with a 5- to 10-s time-out in which the stimulus light was turned on. "Correct rejections," or S− trials on which the animal did not respond in the window of opportunity, were not rewarded. All trials were preceded by a 1-s period designed to ensure separation between individual trials and to ensure that animals had sufficient time to consume the water reward from the previous trial.

Animals generally performed one session per day and were allowed to work until sated. In cases in which two sessions were performed in a day, the first session was halted after 15–20 min and the animal waited a minimum of 1 h before starting the second session. Well-trained animals generally performed 100+ correct trials per day.

Across all 5 animals, over 10,000 total trials were performed (including test pulses and S− trials), with each animal being presented each of the 11 possible stimulus strengths an average of 81 times.

Behavioral data analysis. To prevent the inclusion of trials in which the animal was not highly motivated, trials were excluded from analysis if the animal did not correctly respond to the subsequent test stimulus. Thus a pair of successful responses to test stimuli bracketed each five-trial block. This relatively conservative criterion resulted in the exclusion of ~10% of all trials. Psychometric curves were constructed from the measured behavioral response rates by fitting a sigmoidal curve of the form $P(V) = 1 - (1 - \alpha)e^{-(V/\beta)^{\gamma}}$ where V is the whisker deflection velocity and α, β, and γ are free parameters that were calculated with a nonlinear least-squares regression algorithm in MATLAB. The combined psychometric curve was constructed by pooling the behavioral data from all five animals. Error bars represent 95% confidence intervals. Response times were calculated as the mean time between stimulus onset and the first emitted lick within the response window, limiting the longest possible reaction time to 500 ms. Error bars for the latency data points represent SE.

High-speed videography. High-speed video was used both to map the known air pressure of the chosen range of stimuli to the resulting angular deflection velocities as well as to monitor the effect of whisker motion on detection performance in the awake animal. To prevent self-motion of the animal's whisker pad from affecting the measured velocities resulting from the air puffs, this analysis was performed on an animal under isoflurane anesthesia. While all of the reported behavioral results were obtained in animals in which the full vibrissa array was intact, the vibrissae were subsequently trimmed, leaving only the C row intact in order to facilitate imaging. High-speed video was acquired with an infrared CMOS camera (Fastec InLine 1000 with 1 GB onboard memory). The camera was mounted directly above the animal's head and focused on the whiskers of interest. Backlighting was achieved with two infrared LED arrays (model VQ2121, Lorex Technology) placed ~10 cm below the region of interest; 3/16th-in. opaque white plastic was placed directly above the LEDs to act as a diffuser and to improve the contrast of the whiskers. All video was recorded at either 440 × 330 or 640 × 238 pixels/frame at a temporal resolution of 500 frames/s with exposure time limited to 0.665 ms/frame. The spatial resolution of the region of interest was 7.0–8.5 pixels/mm (Jenks et al. 2010).

All whisker tracking was implemented with a custom routine written in MATLAB. The whisker tracking routine was based on that described by Knutsen et al. (2005), which was subsequently made available online (**http://code.google.com/p/whiskertracker/**). On a subset of videos, results from our custom tracking routine were compared and provided similar results. In the tracking program, three points were chosen on each whisker of interest, one defining the base of the whisker at its junction with the facial pad, one defining a point ~20 mm from the base that defined the length of the whisker that was tracked, and a third intermediate point about which a vertical search was performed on each frame to locate the new position of the whisker. In each frame, a search algorithm was performed in both the positive and negative x (medial-lateral)-directions from the new intermediate point to define the new x- and y-positions of each pixel representing the whisker between two user-defined extremes. Note that this algorithm does not prevent the base of the whisker from moving in the y-direction (rostral-caudal), as it clearly does during self-induced motion of the whisker pad in awake animals. These new x- and y-locations were then fit with a second-order polynomial in each frame. Example frames of the high-speed video with a polynomial fit to the C2 whisker are shown in Fig. 1*C*. The local whisker angle, in degrees, was computed in each video frame by taking the first spatial derivative of the polynomial at the whisker base. Angular velocity was calculated as the change in whisker angle from the previous frame to the current frame, divided by the temporal resolution of the video (2 ms/frame). All results were filtered with a second-order Butterworth low-pass filter with a cutoff frequency of 50 Hz.

Whisker tracking in the anesthetized animal. To calibrate the known stimulus strengths, in pounds per square inch of air pressure, to a more behaviorally relevant range of deflection velocities, the full range of air puff stimuli was applied to an anesthetized animal four times per stimulus. We reasoned that the whisker with the maximum velocity would likely dominate the cortical signal, and thus defined the velocity for a given air puff strength as the maximum deflection velocity observed across all whiskers. In every case, the maximum velocity was measured in the C2 whisker. The maximum velocity for each of the four trials was averaged, resulting in a simple table lookup to convert between air pressure and deflection velocity.

Whisker tracking in the awake animal. After completion of data collection with the full whisker array intact, two animals were continued in the behavioral task with all whiskers excluding the C row trimmed. Analysis was confined to trials in which a 121°/s stimulus was delivered. This value was chosen because it was near the animals' behavioral detection threshold, meaning the animals tended to successfully detect the stimulus on ~50% of the trials. The camera was triggered on stimulus onset and was programmed to record an interval of 500 ms before and after the stimulus presentation. A total of 57 trials were collected across 2 animals.

In the subsequent analysis, the deflection angle as a function of time was measured for the C2 whisker. In all cases, the C2 whisker underwent a larger deflection than other C-row whiskers, and analysis was therefore confined to that whisker alone. For each of the 57 trials, the mean whisker angle in the 150 ms prior to stimulus onset was subtracted from the measured angle, and the discrete Fourier transform of the whisker angle was calculated over the same time interval in MATLAB. Trials were categorized as being either "whisking" or "nonwhisking" trials based on the total power in the 0–15 Hz frequency band, with a hard threshold manually chosen to provide maximum separation. The behavioral response probabilities for these two categories of trial types were compared to assess how the animals' own self-generated whisker motion affected the probability of detecting the stimulus.

Voltage-sensitive dye imaging. Layer 2/3 population activity resulting from whisker deflections was measured in separate animals with VSD imaging, which primarily measures subthreshold membrane voltage fluctuations with high temporal and spatial resolution (Berger et al. 2007; Ferezou et al. 2006; Grinvald and Hildesheim 2004; Petersen et al. 2003a). Two female Sprague-Dawley rats were used for VSD imaging experiments. Surgical procedures were similar to those described above. Anesthesia was induced with isoflurane, then followed by an injection of pentobarbital sodium (Nembutal, 50 mg/kg ip), and a steady depth of anesthesia was maintained throughout the procedure with a continuous delivery of pentobarbital sodium (Nembutal, 12.5 $mg \cdot kg^{-1} \cdot h^{-1}$ iv) through the tail vein. After the skull was cleared of connective tissue, a 3 × 3-mm craniotomy centered at ~2.5 mm caudal to bregma and ~5.5 mm lateral to the midline (Paxinos and Watson 2007) was performed over the barrel cortex, with extreme care taken to avoid heat buildup during the drilling process. An ~1-mm-tall dam was constructed around the craniotomy with dental cement to facilitate the staining process. The bone fragment was then carefully lifted, and the dura was washed with Ringer solution and then dried with a gentle air blow for ~10–15 min or until it had a "glassy" appearance (Lippert et al. 2007). VSD (VSD RH1691, Optical Imaging) was diluted in Ringer solution to 2 mg/ml. The dye solution (~200 μl) was carefully circulated over the cortical surface with a micropipette and was circulated and replenished with a micropipette every 5 min over a total of 2 h, allowing ample time for the dye to diffuse into the cortex. During the entire staining process, the craniotomy was covered whenever possible to avoid premature photobleaching of the dye. After staining, the surface was washed with saline, which was also periodically reapplied during the imaging process to avoid drying.

Imaging was achieved with the use of a 150-W halogen lamp to illuminate the brain surface. The excitation light source was filtered at

621–643 nm, and the fluorescence signals were collected with a MiCam02 camera system (SciMedia, Costa Mesa, CA), which was focused 300 μm below the surface of the cortex, primarily imaging the activity of layer 2/3 neurons. The camera had a frame rate of 200 Hz with a resolution of 192 × 128 pixels comprising a field of view of ~4 mm × 2.5 mm at ×0.63 magnification.

The air puff nozzle was placed in the same position as during the behavioral task, and stimuli were presented to the full whisker array in pseudorandom order for a total of 20 trials at each of the 11 deflection velocities. On each trial, 40 frames (200 ms) and 160 frames (800 ms) were collected before and after stimulus presentation, respectively. The raw fluorescence values at each pixel for each individual trial were recorded with SciMedia software and exported to MATLAB for further analysis.

Voltage-sensitive dye data analysis. All VSD analysis was performed with custom-written scripts in MATLAB. Prior to further analysis, the raw fluorescence data output by the imaging hardware were converted to a normalized value. For each trial, the first 39 frames prior to stimulus onset were averaged together to obtain an average level of background fluorescence, F_0. The background fluorescence was then subtracted from each of the 200 frames in a particular trial to obtain the differential fluorescence, ΔF, and then normalized by the background fluorescence to obtain the standard VSD measure of $\Delta F/F_0$.

Occasionally, large spontaneous waves of activity were observed before stimulus onset that subsequently prevented poststimulus activation. To prevent the inclusion of these trials in the analysis, the activity for the 200 ms prior to stimulus onset was averaged across the entire frame, and any trials in which this prestimulus activity varied by >3 standard deviations from the mean were discarded from the analysis.

Additionally, for visual presentation purposes only, the frames were smoothed with a 3 × 3 boxcar filter, all data below a threshold defined as 10% of the maximum $\Delta F/F_0$ value were removed, and the resulting fluorescence image was superimposed on a background image of the cortical surface. All quantitative analyses were performed on the raw VSD images.

We modeled an observer of cortical activity that was assumed to represent a higher cortical area that may be monitoring primary sensory data to form a decision variable (DV) regarding the presence of a sensory stimulus (Cook and Maunsell 2002). The observer was assumed to have access to activity across a wide area of barrel cortex. To model this, we found the center of mass of activation in the peak frame (generally 40–45 ms after stimulus onset) and, for each frame, averaged the $\Delta F/F_0$ values in a circular region with a radius of 1 mm surrounding this point. Given a barrel diameter of ~300–400 μm, this corresponds to an area of cortex containing the majority of the whisker representations. To account for slow, nonneural changes in the VSD signal, a linear function was fit to the averaged data in this spatial region over the first 200 ms prior to stimulus onset. This linear trend was then subtracted from the entire 1-s trial (Chen et al. 2008).

Accumulation of sensory evidence was modeled by temporally integrating the spatially averaged signal with a leaky window that weighted data from 1 at the current time and decayed exponentially to 0 for past evidence with a time constant of τ. Thus the immediate signal was given the highest weight, and past evidence decayed over time. This model was applied to the measured VSD signal from each individual trial, and the means and standard deviations were calculated for each deflection velocity. To calculate the probability that a stimulus with a particular deflection velocity would be detected by the observer, a detection threshold was chosen, with the response probability measured as the probability of the integrated output crossing that threshold, assuming that the distribution of signals was Gaussian. For a given integration time constant, a range of thresholds were tested to search for the one that produced the lowest mean squared error between the predicted response probabilities and those observed behaviorally. The neurometric decision latency was modeled by generating 1,000 simulated trials based on the mean and standard deviation of the measured responses, with the latency defined as the time at which each integrated response crossed the threshold. Trials in which the signal did not reach the threshold were not included in the latency calculation. These subthreshold trials would correspond with behavioral trials in which insufficient evidence existed to trigger a response, and thus no behavioral latency would exist. The analysis was repeated for a range of time constants from 1 ms up to 1,000 ms, with a new optimal threshold value calculated for each integration time constant.

RESULTS

We trained a total of five head-fixed male Long-Evans rats to perform a go/no-go detection task in which they were required to respond by licking a water spout within a 500-ms window following the onset of a brief puff of air delivered to their full whisker array (Stüttgen et al. 2006; Stüttgen and Schwarz 2008). The strength of the stimulus was varied in each trial to determine how the deflection velocity affected both the probability of response and the reaction time of the animals. The behavioral task is described in detail in METHODS and is shown schematically in Fig. 1, *A* and *B*. Great care was taken to avoid visual, auditory, and non-whisker-mediated tactile cues. The task was performed in a sound- and light-attenuating cubicle with a white noise masking stimulus designed to prevent the animal from cueing on the sound of the air puff stimulus. In addition, an air puff was emitted from a second nearby "distracter nozzle" on a uniform 0- to 5-s random interval. This distracter stimulus was intended to decouple the sound of the air puff and the water reward in case the masking stimulus was not sufficient to fully prevent auditory cues. Catch trials were interleaved to directly measure the chance performance of the animals. The stream of air was carefully aimed to avoid impinging on the animal's face or body. In addition, occasional short sessions were undertaken in which the primary air puff nozzle was aimed slightly above the whisker array. During these sessions, which were kept very short to avoid frustrating the animals, the animals failed to respond reliably to the stimuli, further indicating that they had learned to rely fully upon whisker deflections to perform the task.

Detection performance in the go/no-go task. The five animals in the behavioral portion of the study performed a total of over 10,000 trials during the course of the study. Each animal received an average of 81 presentations of each of the 11 possible stimuli, with the balance of trials consisting of test pulses and catch trials. Figure 2*A* shows lick response rasters and corresponding histograms for three of the tested velocities for a single animal. The light gray section in the lick rasters and histograms designates the enforced no-lick period, during which any licks emitted by the animal resulted in an additional randomized delay of the stimulus. This no-lick period was designed to prevent the animals from licking impulsively. The dark gray section of lick rasters and histograms represents the 500-ms response window, during which the animal was required to respond to receive a water reward. Each tick mark in the lick raster represents the time of contact of the animal's tongue with the water spout. The first lick after the stimulus but within the 500-ms response window resulted in a water reward for the animal and is highlighted (rewarded lick, black). Subsequent licks were generally a result of the animal consuming

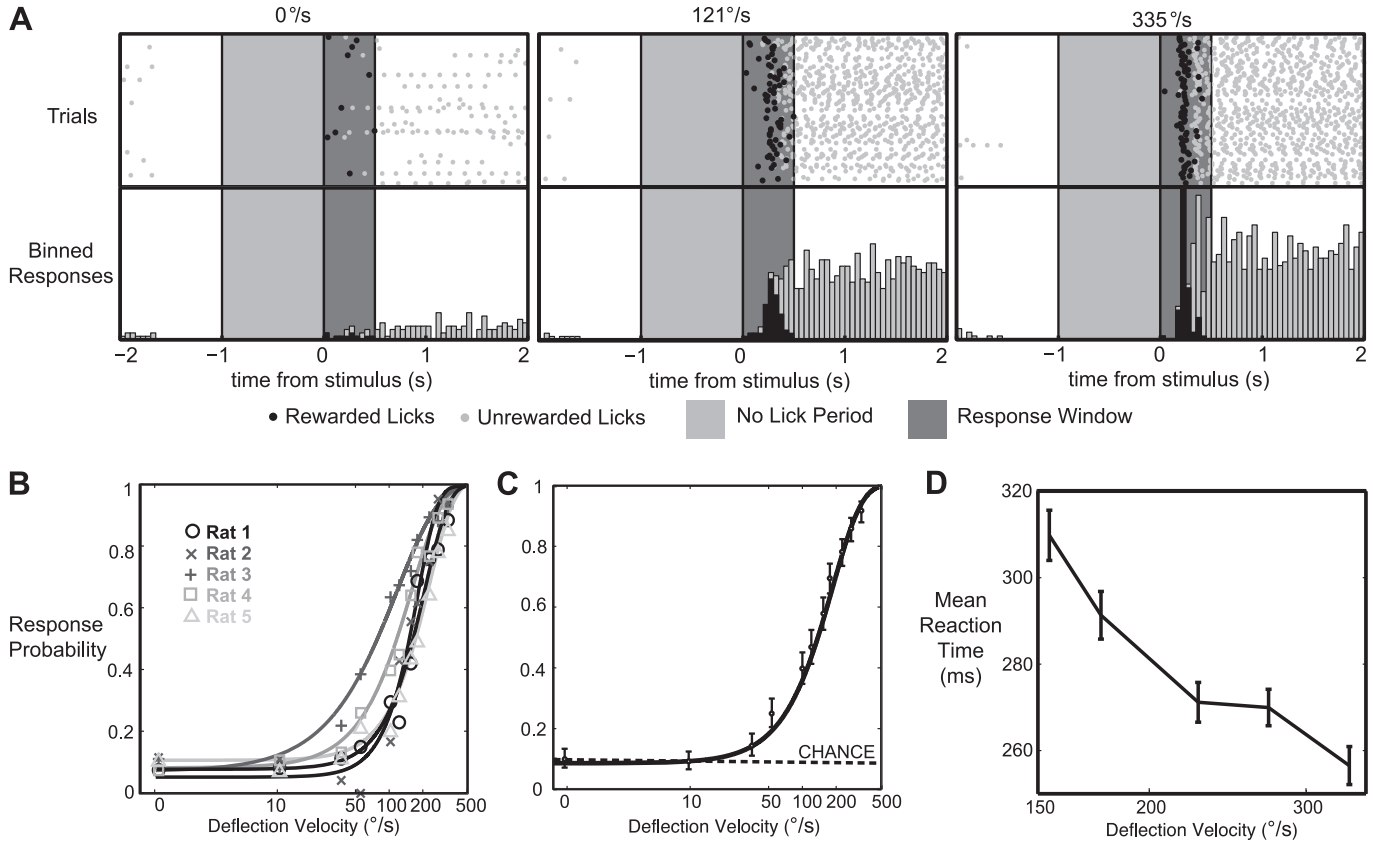

Fig. 2. Response probability increased and reaction time decreased with increasing stimulus strength. *A*: lick response rasters for a single animal for 3 deflection velocities. The light gray region indicates the enforced no-lick period, and the dark gray region indicates the 500-ms response window. Each tick mark in the lick raster indicates the contact of the tongue with the water spout, with all first licks falling within the response window highlighted in black (rewarded lick). The responses are divided into 50-ms bins in the accompanying histograms, with first licks again highlighted in black. *B*: psychometric curves for each of the 5 individual animals. Solid lines represent sigmoidal fits to the response probabilities at each of the 11 tested deflection velocities (see METHODS). Individual mean response probabilities are shown for each of the 5 animals. *C*: psychometric curve for all 5 animals combined. Each data point represents the response probability at a particular deflection velocity with data pooled across all 5 animals. The solid line is the sigmoidal fit to the data, and the dashed horizontal line represents the response probability on catch trials, which is the experimentally derived measure of chance performance. The average detection threshold, which is defined as the deflection strength at which the animals detect the stimulus 50% of the time, was ~125°/s. *D*: mean reaction times for all 5 animals for the 5 highest deflection velocities. There is a 52-ms decrease in the reaction time from the fifth-highest deflection velocity to the highest ($P < 0.005$, 2-sample *t*-test).

the water reward (unrewarded lick, gray). The animals' licking responses were clearly periodic, and subsequent analysis (not shown) indicated an average licking frequency of ~8 Hz. Figure 2*B* shows the individual response probabilities as a function of deflection velocity for each of the five animals in the study. Each of the five animals showed a maximal response probability of ~90% for the highest velocity and responded to ~10% of the 0°/s stimuli, in which no stimulus was applied. It should be noted that the 0°/s stimuli were distinct from the catch trials, which are described in detail below, in that the primary stimulus solenoid was opened on 0°/s trials but there was no air pressure present in the line.

Figure 2*C* shows the psychometric curve for the combined data among all five animals. The dashed horizontal line labeled "chance" in Fig. 2*C* represents the averaged response probability on catch trials, which were trials in which no tactile stimulus was delivered but the distracter nozzle was fired at the time of the stimulus. Responses on catch trials were considered false alarms and were penalized with a 5- to 10-s time-out period in which the stimulus light in the behavioral chamber was turned on. The average response rate for all catch trials was 9.74% (13.66%, 11.39%, 8.70%, 12.77%, and 6.67% for *rats 1–5*, respectively), which corresponded well with the response rate on 0°/s trials (9.69%), further indicating that the animals were not using auditory cues to detect the presence of a stimulus. Assuming that the animals' tendency to guess at the presence of a stimulus remained constant throughout the duration of the trial, a theoretical chance response rate can be calculated by dividing the length of the response window (500 ms) by the overall duration in which a correct guess could result in a reward, which was 4.5 s. This yields an expected chance performance level of 11.11%, which also corresponds well with the experimentally measured chance performance.

Figure 2*D* shows the mean reaction times for the highest five velocities tested for all five of the animals in this study. The mean reaction time at the threshold velocity, 154°/s, was 309 ms, and the reaction time steadily decreased with increasing stimulus strength. The reaction time at the highest velocity, 335°/s, was 257 ms. This 52-ms difference between the strongest deflection velocity and the threshold level deflection velocity was statistically significant ($P < 0.005$, 2-sample *t*-test). Reaction times for subthreshold deflection velocities, in which the animals tended to respond on less than half of the trials, were much more variable and were therefore not plotted.

Detection in the presence of self-motion. Rats and other rodents possess fine control over the motion of their whiskers

and often explore their environment with a rhythmic sweeping of their vibrissae known as whisking. Multiple studies have shown that whisking corresponds with changes in the processing state of cortex, leading to a reduction in the cortical response to passively applied stimuli (Castro-Alamancos 2004; Crochet and Petersen 2006; Fanselow and Nicolelis 1999; Ferezou et al. 2006, 2007). Through use of high-speed video, we sought to explicitly determine whether self-induced whisker motion affected the animals' probability of detecting the externally applied stimulus. After the completion of data collection with the full vibrissa array intact, two animals continued to perform the task with only the central C row of whiskers intact and all others trimmed at skin level, in order to facilitate imaging. The whiskers were backlit with infrared LEDs (Jenks et al. 2010), and the camera was positioned directly above the head of the animal. The angle at the base of the whisker was subsequently evaluated with a custom MATLAB routine (see METHODS for details on the videography and whisker tracking).

To maximize the possibility of recording both correct and incorrect trials, the camera was only triggered on presentation of 121°/s stimuli, which was just below the behavioral detection threshold (response probability with full vibrissa array intact = 46.58%). A total of 57 trials were recorded across the 2 animals. Trials were separated into two categories based on the amount of whisker motion in the 150-ms epoch prior to stimulus delivery: those with high power in the 0–15 Hz range, which were categorized as whisking trials, and those with low power in the 0–15 Hz range, which were categorized as nonwhisking trials. Figure 3*A* shows an example of both types of trials, from 450 ms prior to stimulus onset to 200 ms after stimulus onset. Figure 3*B* shows the mean ± 1 standard deviation of the power from 0 to 75 Hz for all of the whisking and nonwhisking trials and clearly demonstrates a distinct separation between the two categories in the 0–15 Hz range. Figure 3*B*, *inset*, shows the angle vs. time traces for the 150 ms prior to stimulus onset for all of the whisking and nonwhisking trials, with trials in which the animal correctly detected the stimulus shown in black and those in which the animal failed to detect the stimulus shown in gray. The behavioral response probabilities for both types of trials are shown in Fig. 3*C*, demonstrating that the animals had a significantly higher response rate on trials in which whisker motion was suppressed in the 150 ms prior to the arrival of the stimulus ($P = 0.0313$, Wilcoxon rank sum test). To determine whether or not the change in response probabilities represents a change in the signal or noise distributions, a change in the animals' response criterion, or some combination of these factors, both the hit rate and the false alarm rates must be considered. While we did not record high-speed video during presentations of catch stimuli to directly measure false alarm probability on these trials, an alternative measure of the animals' response criterion is their propensity to emit an anticipatory lick prior to stimulus presentation, resulting in a subsequent delay of the stimulus. The animals emitted an anticipatory lick on 3 of 17 (17.6%) of the whisking trials and 4 of 40 (10.0%) of the nonwhisking trials, representing a nonsignificant difference in the rate of anticipatory licking across the two trial types ($P = 0.4340$, Wilcoxon rank sum test). This suggests that the reduced response probabilities represented a change in the way the stimulus was perceived in the whisking and nonwhisking conditions, as opposed to a change in the attentional or motivational state of the animals.

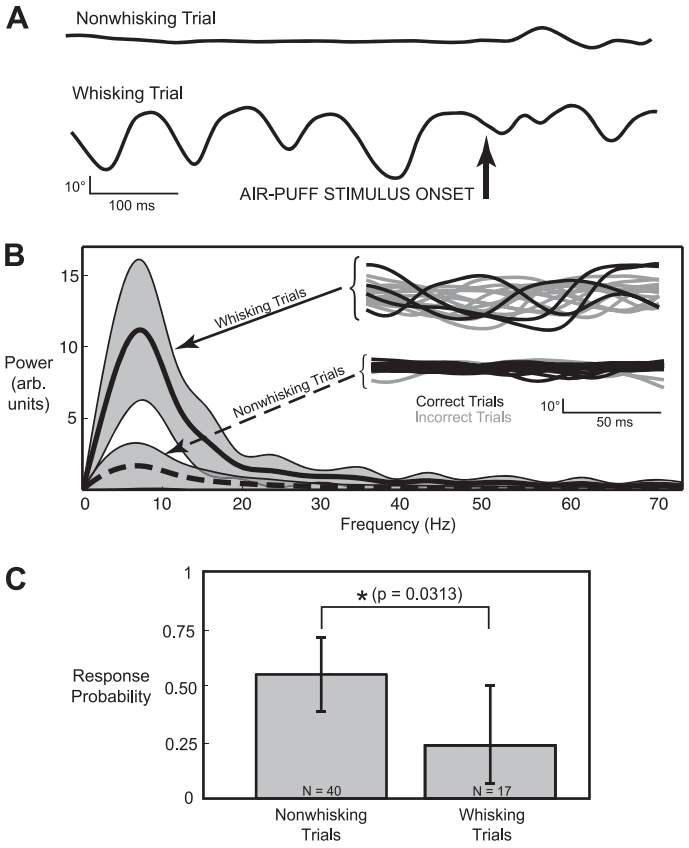

Fig. 3. Self-motion of whiskers degrades detection performance. In a subset of behavioral trials, the whiskers were trimmed, leaving only the C row to facilitate imaging. High-speed video was collected during presentation of the 121°/s stimulus, which corresponded to the velocity at which the animals responded correctly on 45% of the trials with the full vibrissa array intact. *A*: whisker angle at the base was measured with custom tracking software, and trials were categorized based on the total power in the 0–15 Hz frequency band. Shown are representative examples of both a nonwhisking and a whisking trial. *B*: average power for all of the whisking (solid line) and nonwhisking (dashed line) trials in the 150 ms prior to stimulus onset, with the shaded region representing 1 standard deviation about the mean. *Inset* shows all of the whisking trials (*top*) and all of the nonwhisking trials (*bottom*). Behaviorally correct and incorrect trials are black and gray, respectively. *C*: the response probability was significantly higher during periods of reduced self-motion prior to the arrival of the stimulus. Response probabilities for the 2 conditions were 0.55 and 0.24, respectively. Error bars represent 95% confidence intervals. *Statistical significance between the response probabilities under the 2 conditions ($P = 0.0313$, Wilcoxon rank sum test).

Voltage-sensitive dye imaging of cortical activation. In additional experiments in the anesthetized rat, VSD imaging was used to characterize the population cortical response resulting from the range of whisker deflection velocities applied during the behavioral task. VSD imaging has previously been shown to capture primarily subthreshold membrane potential fluctuations in layer 2/3 pyramidal neurons (Berger et al. 2007; Ferezou et al. 2006; Petersen et al. 2003a). Figure 4*A* shows a schematic of the VSD imaging setup. The air puff nozzle was positioned as in the behavioral task, and deflections were applied to the entire vibrissa array. Images of the resulting layer 2/3 cortical activation were captured at 200 Hz, with each stimulus applied 20 times in pseudorandom order. Figure 4*B* shows sample frames for five of the applied deflection velocities from 15 ms to 55 ms after the stimulus presentation. The

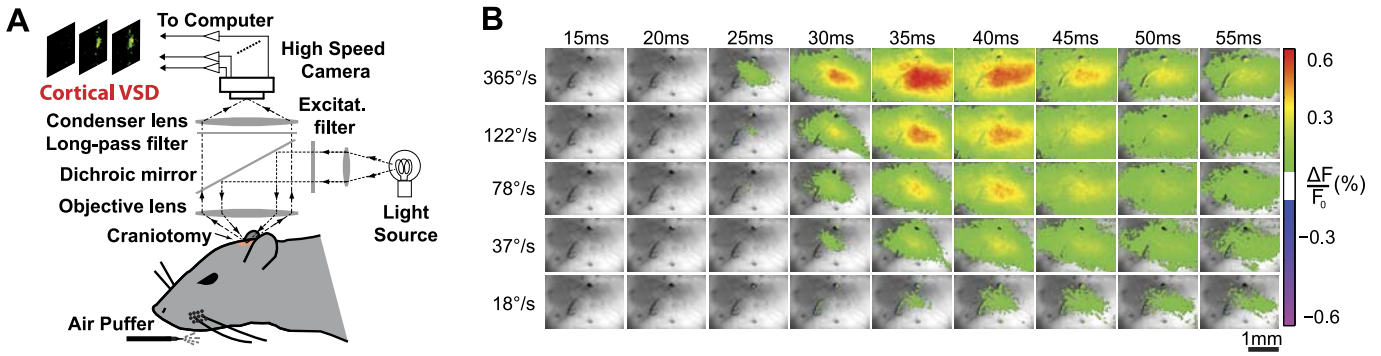

Fig. 4. Voltage-sensitive dye (VSD) imaging was used to characterize the layer 2/3 cortical population response to the air puff stimuli. *A*: schematic of the VSD system. After a craniotomy was performed over the barrel cortex, VSD RH1691 was allowed to diffuse into the cortex. A high-speed camera was subsequently focused 300 μm below the cortical surface, and images of cortical surface were captured every 5 ms. *B*: image frames showing the spatiotemporal evolution of the signal during the 55 ms after stimulus onset for 5 stimulus strengths. Frames representing the initial 15 ms are not shown. Background image shows the region of cortex being imaged. Responses were smoothed with a 3 × 3 boxcar filter, and any response <10% of the maximum value was excluded for visualization purposes. $\Delta F/F_0$, differential fluorescence normalized to background fluorescence.

images represent the average of all 20 stimulus presentations at each deflection velocity, and the activity was thresholded at 10% of the peak fluorescence value, smoothed, and overlaid on an image of the cortical surface for visualization purposes. All subsequent quantitative analyses used the raw VSD signal. In the case of the higher-velocity stimuli, activity was initially seen to be present by the 25 ms frame, although it appeared 5–10 ms later for the weaker stimuli. In all cases, the signal initially grew in both magnitude and spatial extent before slowly decaying back to baseline. The spatiotemporal dynamics of the VSD signal, as well as the relationship between increasing signal strength and response magnitude, were largely consistent with previous VSD imaging literature (Berger et al. 2007; Petersen et al. 2003a, 2003b).

Past studies have indicated that sensory detection can be well modeled as a thresholding of the spatial and temporal integration of ongoing, noisy sensory information (Carpenter 2004; Chen et al. 2008; Cook and Maunsell 2002; Fridman et al. 2010; Gold and Shadlen 2007, 2001; Huk and Shadlen 2005; Mazurek et al. 2003; Roitman and Shadlen 2002; Schall and Thompson 1999; Smith and Ratcliff 2004; Stüttgen and Schwarz 2010). Spatially, we integrated the VSD signal within a 1-mm radius of the center of mass of activity in the peak frame, resulting in an area of the primary sensory cortex containing the representation of the majority of the barrel cortex. Figure 5*A* shows the trial-by-trial activity inside the included region of the barrel cortex, with the averaged frames from 15 ms to 90 ms shown above. In the averaged frames, only the activity within the 1-mm radius is shown. While precise details of the temporal integration process vary somewhat among studies, most have modeled the accumulation of sensory evidence with a leaking integrator with a time constant in the range of tens to hundreds of milliseconds. Here, we systematically evaluated a range of window sizes and shapes but found that the results were largely invariant to the shape of the window. We therefore utilized the conventional exponentially decaying window with time constant τ. Figure 5*B* shows the output of the integrator with a time constant of 20 ms for two deflection velocities, with blue being the highest-velocity (335°/s) stimulus and green being the 154°/s, near threshold-level stimulus. The solid lines represent the means of the integrated outputs, and the shaded regions represent one standard deviation about the mean. A neurometric detection threshold was chosen, and the probability of response for a particular deflection velocity was calculated as the probability that the integrated signal crossed this threshold. A range of detection threshold values were systematically tested with the goal of finding the threshold that minimized the mean squared error between the predicted and behaviorally observed response probabilities. The optimal threshold is shown as a dashed line in Fig. 5*B*. Figure 5*C* shows the predicted detection probabilities, shown as red circles, for all 11 of the whisker deflection velocities used in the behavioral study, averaged across the 2 animals in the acute portion of the study. The behaviorally observed detection probabilities (from Fig. 2*C*) are again shown as for comparison. The black curve is the sigmoidal fit to the behavioral response probabilities, and the red curve is the sigmoidal fit to the predicted response probabilities. After the optimal detection threshold was determined for each integration time constant, the neurometric decision latencies were modeled as the threshold crossing times generated from the distribution of the integrated VSD signal (see METHODS). Trials in which the signal did not cross the threshold were excluded from the latency calculation. Figure 5*D* shows the predicted neurometric response latencies using an integration window with a 20-ms time constant. Figure 5*E* shows that, as expected, the latencies of the VSD threshold crossing times were significantly shorter than the corresponding behavioral reaction times (Fig. 2*D*), and the absolute difference in latencies between the strongest stimulus and the threshold stimulus was significantly smaller than that of the behavioral reaction time (7–8 ms vs. 40–50 ms). However, the relative changes in the corresponding latencies induced by the strongest stimulus and the threshold stimulus were also evaluated for both the VSD recordings and the behavior. As shown in Fig. 5*E*, *bottom*, despite the differences in absolute measures between the psychometric and neurometric latencies, the relative measures were much more consistent between the cortical recordings and behavior.

DISCUSSION

The present study was designed to allow us to address four primary issues. First, in a head-fixed behavioral detection task in which multiple whiskers were deflected, we sought to determine the relationship between whisker deflection velocity and the probability that the animal could successfully detect the applied stimulus. Simultaneously, by allowing the animals to respond as quickly as possible, we were able to demonstrate a

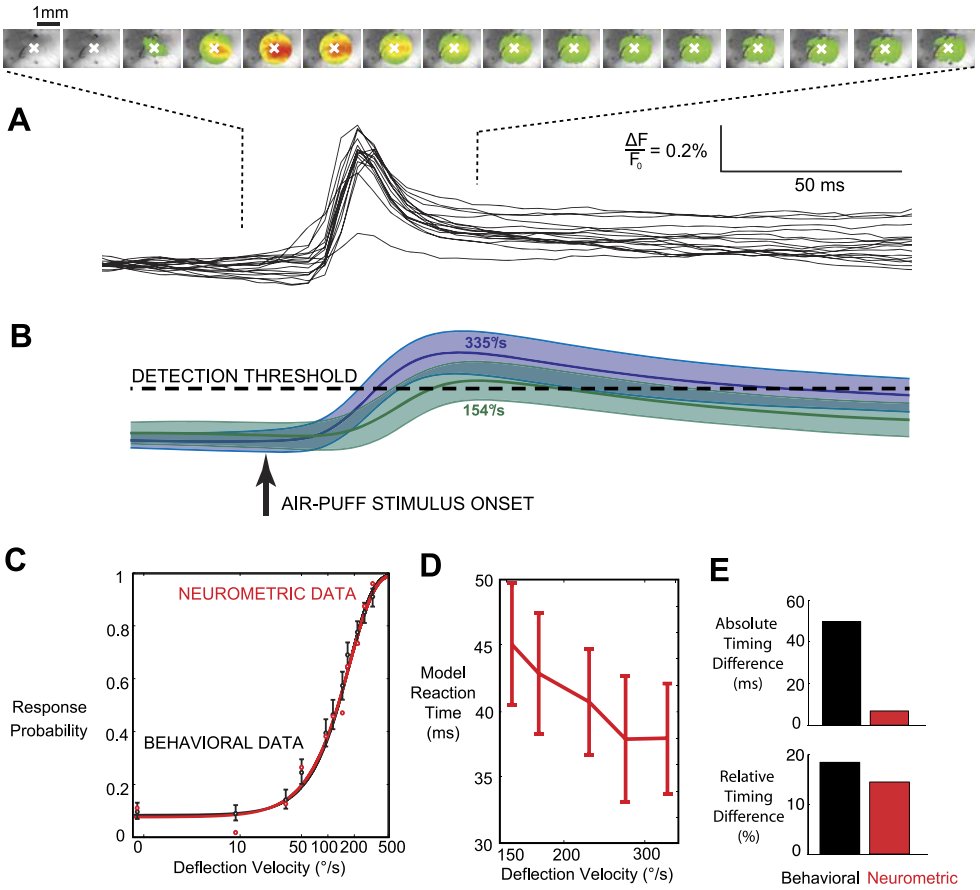

Fig. 5. Neurometric performance based on an accumulating evidence model of the VSD signal predicts psychometric performance. *A*: a circular area with a radius of 1 mm centered at the center of mass of the peak signal, designated with a white X, was treated as the input to the accumulating evidence model. Shown are the averaged responses to the strongest air puff stimulus from 15 to 100 ms, with only the signal inside the region of interest shown. Below is the spatial average of these frames for each of the individual trials. *B*: the neurometric signal is generated from leaky integration of the VSD signal from *A*. Specifically, the VSD signal was convolved with an exponential window with a time constant of 20 ms. Shown are the mean and standard deviation of the integrated response for the strongest (335°/s, shown in purple) and the fifth-strongest (154°/s, shown in cyan) velocities. For a given detection threshold, the probability of crossing that threshold was calculated for each of the 11 deflection strengths. The value of the threshold was chosen to minimize the mean squared error between the calculated response probabilities and those measured behaviorally (Fig 2*C*). *C*: the neurometric-psychometric match using the optimized threshold values. The neurometric data points represent the average across 2 animals. *D*: the neurometric latencies were measured as the time that each integrated population response crossed the optimized threshold. Note that responses that fail to reach the threshold are not included in the measured neurometric latency. *E*: comparison of both the total change in latencies and the % change in latencies from the strongest presented stimulus to the threshold-level stimulus. Black bars represent the values measured from the behaving animals, and red bars represent the output of the accumulating evidence model. The absolute change in neurometric latency is not reflective of the absolute change in the animals' reaction times, but the relative change provides much closer correspondence.

relationship between the stimulus strength and the mean reaction times of the animals in the task. The animals were then allowed to continue the task with only a single row of their whiskers remaining, allowing us to collect high-speed video of their vibrissae during presentation of threshold-level stimuli to determine the effect that whisker motion prior to stimulus onset had on the probability of detecting the stimulus. Finally, VSD imaging of the barrel cortex was used to characterize the population cortical response to the whisker deflections used in the behavioral task and to explore a candidate neural coding scheme that could explain both the observed response probabilities and reaction times.

Detectability of velocity transients in a tactile input. In the tasks utilized in this study, the behavioral performance is reported in terms of the angular velocity of the vibrissae as calibrated through high-speed video under controlled conditions in anesthetized animals. When an object makes contact with a rodent's whisker, the motion of the whisker is transmitted to the densely innervated follicle at the whisker base, giving rise to complex mechanics that have only recently been investigated in detail (Birdwell et al. 2007; Towal et al. 2011). Electrophysiological studies at the thalamic and cortical levels have largely focused on the neuronal responses to velocity and amplitude of simple tactile stimuli (Boloori et al. 2010; Lee and Simons 2004; Temereanca et al. 2008; Wang et al. 2010). Although both the amplitude and velocity of a whisker deflection can covary, multiple studies have indicated that it is primarily the velocity of the whisker deflection that is ultimately encoded at the level of the primary sensory cortex (Boloori et al. 2010; Pinto et al. 2000). As a first step, we have therefore focused on the velocity of the applied stimuli when measuring the animals' response probabilities and reaction times, although both velocity and amplitude were seen to increase with increased stimulus strength and other dynamical measures are also possibly important. This analysis yielded a detection threshold, defined as the velocity at which the animals responded with 50% probability, of ~125°/s. This threshold value is approximately half of that measured in a very

similar head-fixed detection task in which only a single whisker was deflected with a piezoelectric actuator (Stüttgen and Schwarz 2008). This difference can largely be accounted for by the fact that our stimuli were applied to the entire intact vibrissa array, allowing multiple whiskers to encode the stimulus simultaneously, which has previously been shown to increase the magnitude of the cortical response to a given stimulus in anesthetized animals (Mirabella et al. 2001). It should be noted that although the central data reported here correspond to the full vibrissa array, it is our observation that the nozzle used to deliver the air puff stimulus produced a fairly focused stream of air that was largely limited to a single row of vibrissae, and thus the data obtained from vibrissa arrays trimmed to a single row were not significantly different from data obtained with the intact array. Furthermore, in an aperture discrimination task, in which animals were freely moving, the ability of rats to discriminate between apertures of similar widths was severely degraded when <8–12 whiskers on a given side of the face were intact (Krupa et al. 2001), and animals performing a texture discrimination task required at least 2 whiskers per side to accurately perform the task (Carvell and Simons 1995), suggesting that integration across the vibrissa array could account for the lower detection threshold we observed here.

Suppression of self-motion improves detection performance. When rats are engaged in active exploration of their environments, or are trained in a task that requires active palpation of an object, they generally engage in a 5- to 15-Hz rhythmic sweeping motion of their whiskers known as whisking (Berg and Kleinfeld 2003; Bermejo et al. 2002; Brecht et al. 1997; Carvell and Simons 1990; Gustafson and Felbain-Keramidas 1977). However, in some behaviors or tasks self-generated whisker motion may actually be detrimental in providing accurate tactile feedback. For example, rats in locomotion-based aperture discrimination tasks (Krupa et al. 2001, 2004), engaged in wall following (Jenks et al. 2010; Milani et al. 1989), or performing passive detection tasks under head fixation (Stüttgen et al. 2006) have been anecdotally reported to avoid self-motion of the whiskers.

Here, using video analysis of the whisker motion while rats were engaged in the detection task, we demonstrated not only that rats held their whiskers still during a majority of trials but that their probability of accurately detecting the stimulus was actually decreased on trials in which they engaged in active motion of the whiskers.

This result corresponds well with other studies showing that the cortical response to peripheral inputs is attenuated when the animal is whisking (Castro-Alamancos 2004; Crochet and Petersen 2006; Fanselow and Nicolelis 1999; Ferezou et al. 2006, 2007; Hentschke et al. 2006; Poulet et al. 2012). This attenuation, combined with a shift to a more desynchronized cortical state (Poulet et al. 2012), could inherently reduce the probability of detecting a weak, passively applied stimulus. Additionally, we have previously demonstrated in the anesthetized animal that repetitively applied whisker movements place the cortex in an adapted state that proves detrimental for the detection of subsequent stimuli (Wang et al. 2010). Although the extent to which adaptation exists in the awake animal appears to be less than in the anesthetized animal (Castro-Alamancos 2004), attenuation due to adaptation would also likely serve to diminish detection performance. It has been shown that the pathway encodes information directly related to whisker motion, even when the whiskers are not in contact with an object (Khatri et al. 2009; Leiser and Moxon 2007; Yu et al. 2006). An alternative explanation for the reduced response probability, therefore, could be that the neural activity resulting from whisking could overwhelm that resulting from the stimulus itself, effectively decreasing the signal-to-noise ratio and degrading detection performance. Finally, the animals' attentional or motivational state could be different in the two cases, with trials in which the animal is whisking corresponding to epochs in which the animal is simply less attendant to the task. Although our data set indicates that the response criterion is not significantly different in the two behavioral states, none of the above scenarios, or interactions thereof, can be ruled out without both a more complete measure of false-alarm response probabilities and simultaneous recordings of cortical activity. While we cannot necessarily conclude that the suppression of whisking is an active strategy employed by the animals in our task, the results here indicate that in tasks where the animal must detect a weak, transient stimulus the animal must balance incoming activity resulting from self-generated motion with that resulting from the stimulus itself.

VSD imaging of cortex in the anesthetized animal predicts performance in behaving animals. According to the "sequential analysis framework" of decision making, sensory evidence about the presence of a stimulus is built up over time and compared with an internally determined threshold (Gold and Shadlen 2007). This would allow the brain to respond quickly to a strong, unambiguous stimulus but would require a longer integration period for weaker inputs. The VSD signal provides an excellent measure of the subthreshold population activity in layer 2/3 of the barrel cortex with good temporal resolution (Berger et al. 2007; Ferezou et al. 2006; Petersen et al. 2003a), thereby providing us with access to the signal that likely represents sensory evidence in the behaving animal, including the trial-to-trial variability (Petersen et al. 2003b), which might help to explain the variability both in the animals' response probabilities and in the timing of their responses. As in any sensory pathway, it is not currently known where the percept of a tactile input actually occurs in the vibrissa pathway, but lesion studies indicate that primary somatosensory cortex (S1) is necessary for simple sensory tasks such as the detection of a whisker contact (O'Connor et al. 2010a), and it is thus not mediated entirely in subcortical structures. Our observer was modeled as an exponentially leaky integrator with access to the averaged signal over a broad area of barrel cortex. The model contained two important parameters that could be adjusted to provide a fit between the output of the integrator and the observed behavioral results: the time constant of integration and the threshold above which the neural signal must pass to trigger a response. For a particular time constant, choosing the proper threshold was especially critical to avoid either including too many false alarms if set too low or missing too many low-velocity stimuli if set too high. During task performance, the animals would likely dynamically adjust this threshold based on their motivation to correctly perform the task, and our model threshold would represent an average threshold used by the animals in the task.

We tested a range of time constants from 1 ms up to 1,000 ms in our model but found that the best fit between the predicted and behavioral response probabilities was achieved

with a time constant of 20 ms. This corresponds well with another recent study of temporal integration in the whisker system of rats engaged in a vibrotactile detection task, in which an integrator with a similarly short time constant provided a good match between the observed behavioral results and the recorded single-unit activity (Stüttgen and Schwarz 2010).

The behavioral task was designed such that the animals had a short window in which to respond to the onset of the stimulus in order to receive a water reward on a given trial. This incentive to respond quickly was tempered with a relatively long time-out period in the event of a false alarm. As shown in Fig. 2*D*, this led to a decreasing reaction time with increasing stimulus velocity, with a 52-ms difference in mean reaction times between the threshold level deflection velocity and the maximum tested deflection velocity. This represents a 17% decrease in reaction times from the highest-velocity stimulus to the threshold-level stimulus. If the output of the integrator was assumed to represent the final DV, it might be expected that the range of times at which the integrated signal crossed the detection threshold would display a similar 52-ms difference. Alternatively, if the output of the integrator is instead assumed to represent an early stage of the decision making process, it might be expected that the stronger, faster signals would continue to propagate more quickly. In this case, the percent difference in neural reaction times would be expected to match, as opposed to the raw difference. Indeed, as shown in Fig. 5*E*, the measured reaction times match much more closely in percent change (16% change in the model reaction times) than in absolute terms. However, studies in the somatosensory (Luna et al. 2005) and visual (Cook and Maunsell 2002; Chen et al. 2006) systems of primates have estimated integration time constants in the hundreds of milliseconds with a similar exponentially leaking integrator of primary sensory information. The possibility remains that animals in our task could be integrating information over a similarly long timescale. Our simulations showed that doing so would both increase and spread out the neural reaction times, leading to a much closer match in the absolute latencies, but at the expense of accuracy in predicting the response probabilities.

Taken together, the results here show that the behavioral performance of the animal in simple tasks is well predicted by measurements of spatiotemporal cortical activation in parallel experiments in the anesthetized animal, despite the likely differences related to brain state. The approach further provides a potential framework for the evaluation of spatiotemporal cortical signaling in more complex tasks that require discriminability between disparate sensory inputs, or for tasks that require more complex combinations of detection and discrimination.

ACKNOWLEDGMENTS

The authors thank Cornelius Schwarz for assistance in designing the behavioral experiments as well as for feedback during the preparation of the manuscript. We also thank Clare Gollnick and He Zheng for valuable discussions throughout the project.

GRANTS

This work was supported by National Institute of Neurological Disorders and Stroke Grant 2R01-NS-048285 to G. B. Stanley. D. R. Ollerenshaw is supported by National Institutes of Health Ruth L. Kirschstein National Research Service Award F31-NS-074797. B. A. Bari received support from a Georgia Institute of Technology Petit Undergraduate Research Scholarship and a President's Undergraduate Research Award. D. C. Millard is supported by a National Science Foundation Graduate Research Fellowship.

DISCLOSURES

No conflicts of interest, financial or otherwise, are declared by the author(s).

AUTHOR CONTRIBUTIONS

Author contributions: D.R.O., L.E.O., Q.W., and G.B.S. conception and design of research; D.R.O., B.A.B., D.C.M., L.E.O., and Q.W. performed experiments; D.R.O. and B.A.B. analyzed data; D.R.O., B.A.B., Q.W., and G.B.S. interpreted results of experiments; D.R.O. prepared figures; D.R.O. and G.B.S. drafted manuscript; D.R.O., B.A.B., D.C.M., L.E.O., Q.W., and G.B.S. edited and revised manuscript; D.R.O., B.A.B., D.C.M., L.E.O., Q.W., and G.B.S. approved final version of manuscript.

REFERENCES

Adibi M, Arabzadeh E. A comparison of neuronal and behavioral detection and discrimination performances in rat whisker system. *J Neurophysiol* 105: 356–365, 2011.

Adibi M, Diamond ME, Arabzadeh E. Behavioral study of whisker-mediated vibration sensation in rats. *Proc Natl Acad Sci USA* 109: 971–976, 2012.

Ahissar E, Sosnik R, Haidarliu S. Transformation from temporal to rate coding in a somatosensory thalamocortical pathway. *Nature* 406: 302–306, 2000.

Berg RW, Kleinfeld D. Rhythmic whisking by rat: retraction as well as protraction of the vibrissae is under active muscular control. *J Neurophysiol* 89: 104–117, 2003.

Berger T, Borgdorff A, Crochet S, Neubauer FB, Lefort S, Fauvet B, Ferezou I, Carleton A, Lüscher HR, Petersen CCH. Combined voltage and calcium epifluorescence imaging in vitro and in vivo reveals subthreshold and suprathreshold dynamics of mouse barrel cortex. *J Neurophysiol* 97: 3751–3762, 2007.

Bermejo R, Vyas A, Zeigler HP. Topography of rodent whisking. I. Two-dimensional monitoring of whisker movements. *Somatosens Motor Res* 19: 341–346, 2002.

Birdwell JA, Solomon JH, Thajchayapong M, Taylor MA, Cheely M, Towal RB, Conradt J, Hartmann MJZ. Biomechanical models for radial distance determination by the rat vibrissal system. *J Neurophysiol* 98: 2439–2455, 2007.

Boloori AR, Jenks RA, Desbordes G, Stanley GB. Encoding and decoding cortical representations of tactile features in the vibrissa system. *J Neurosci* 30: 9990–10005, 2010.

Brecht M, Preilowski B, Merzenich MM. Functional architecture of the mystacial vibrissae. *Behav Brain Res* 84: 81–97, 1997.

Britten KH, Shadlen MN, Newsome WT, Movshon JA. The analysis of visual motion: a comparison of neuronal and psychophysical performance. *J Neurosci* 12: 4745–4765, 1992.

Carpenter R. Contrast, probability, and saccadic latency: evidence for independence of detection and decision. *Curr Biol* 14: 1576–1580, 2004.

Carvell GE, Simons D. Biometric analyses of vibrissal tactile discrimination in the rat. *J Neurosci* 10: 2638–2348, 1990.

Carvell GE, Simons DJ. Task- and subject-related differences in sensorimotor behavior during active touch. *Somatosens Motor Res* 12: 1–9, 1995.

Castro-Alamancos MA. Absence of rapid sensory adaptation in neocortex during information processing states. *Neuron* 41: 455–464, 2004.

Chen Y, Geisler WS, Seidemann E. Optimal temporal decoding of neural population responses in a reaction-time visual detection task. *J Neurophysiol* 99: 1366–1379, 2008.

Cook EP, Maunsell JHR. Dynamics of neuronal responses in macaque MT and VIP during motion detection. *Nat Neurosci* 5: 985–994, 2002.

Crochet S, Petersen CCH. Correlating whisker behavior with membrane potential in barrel cortex of awake mice. *Nat Neurosci* 9: 608–610, 2006.

Curtis JC, Kleinfeld D. Phase-to-rate transformations encode touch in cortical neurons of a scanning sensorimotor system. *Nat Neurosci* 12: 492–501, 2009.

Derdikman D, Hildesheim R, Ahissar E, Arieli A, Grinvald A. Imaging spatiotemporal dynamics of surround inhibition in the barrels somatosensory cortex. *J Neurosci* 23: 3100–3105, 2003.

Diamond ME, von Heimendahl M, Knutsen PM, Kleinfeld D, Ahissar E. "Where" and "what" in the whisker sensorimotor system. *Nat Rev Neurosci* 9: 601–612, 2008.

Fanselow EE, Nicolelis MAL. Behavioral modulation of tactile responses in the rat somatosensory system. *J Neurosci* 19: 7603–7316, 1999.

Ferezou I, Bolea S, Petersen CCH. Visualizing the cortical representation of whisker touch: voltage-sensitive dye imaging in freely moving mice. *Neuron* 50: 617–629, 2006.

Ferezou I, Haiss F, Gentet LJ, Aronoff R, Weber B, Petersen CCH. Spatiotemporal dynamics of cortical sensorimotor integration in behaving mice. *Neuron* 56: 907–923, 2007.

Fridman GY, Blair HT, Blaisdell AP, Judy JW. Perceived intensity of somatosensory cortical electrical stimulation. *Exp Brain Res* 203: 499–515, 2010.

Gerdjikov TV, Bergner CG, Stüttgen MC, Waiblinger C, Schwarz C. Discrimination of vibrotactile stimuli in the rat whisker system: behavior and neurometrics. *Neuron* 65: 530–540, 2010.

Gold JI, Shadlen MN. The neural basis of decision making. *Annu Rev Neurosci* 30: 535–574, 2007.

Gold JI, Shadlen MN. Neural computations that underlie decisions about sensory stimuli. *Trends Cogn Sci* 5: 10–16, 2001.

Grinvald A, Hildesheim R. VSDI: a new era in functional imaging of cortical dynamics. *Nat Rev Neurosci* 5: 874–885, 2004.

Guic-Robles E, Valdivieso C, Guajardo G. Rats can learn a roughness discrimination using only their vibrissal system. *Behav Brain Res* 31: 285–289, 1989.

Gustafson JW, Felbain-Keramidas SL. Behavioral and neural approaches to the function of the mystacial vibrissae. *Psychol Bull* 84: 477–488, 1977.

Hartmann MJ, Johnson NJ, Towal RB, Assad C. Mechanical characteristics of rat vibrissae: resonant frequencies and damping in isolated whiskers and in the awake behaving animal. *J Neurosci* 23: 6510–6519, 2003.

Hayar A, Bryant JL, Boughter JD, Heck DH. A low-cost solution to measure mouse licking in an electrophysiological setup with a standard analog-to-digital converter. *J Neurosci Methods* 153: 203–207, 2006.

Hentschke H, Haiss F, Schwarz C. Central signals rapidly switch tactile processing in rat barrel cortex during whisker movements. *Cereb Cortex* 16: 1142–1156, 2006.

Huk AC, Shadlen MN. Neural activity in macaque parietal cortex reflects temporal integration of visual motion signals during perceptual decision making. *J Neurosci* 25: 10420–10436, 2005.

Hutson K, Masterton R. The sensory contribution of a single vibrissa's cortical barrel. *J Neurophysiol* 56: 1196–1223, 1986.

Jacobs AL, Fridman G, Douglas RM, Alam NM, Latham P. Ruling out and ruling in neural codes. *Proc Natl Acad Sci USA* 106: 5936–5941, 2009.

Jenks RA, Vaziri A, Boloori AR, Stanley GB. Self-motion and the shaping of sensory signals. *J Neurophysiol* 103: 2195–2207, 2010.

Khatri V, Bermejo R, Brumberg JC, Keller A, Zeigler HP. Whisking in air: encoding of kinematics by trigeminal ganglion neurons in awake rats. *J Neurophysiol* 101: 1836–1846, 2009.

Knutsen PM, Derdikman D, Ahissar E. Tracking whisker and head movements in unrestrained behaving rodents. *J Neurophysiol* 93: 2294–2301, 2005.

Krupa DJ, Matell MS, Brisben AJ, Oliveira LM, Nicolelis MAL. Behavioral properties of the trigeminal somatosensory system in rats performing whisker-dependent tactile discriminations. *J Neurosci* 21: 5752–5763, 2001.

Krupa DJ, Wiest MC, Shuler MG, Laubach M, Nicolelis MAL. Layer-specific somatosensory cortical activation during active tactile discrimination. *Science* 304: 1989–1992, 2004.

Lee SH, Simons DJ. Angular tuning and velocity sensitivity in different neuron classes within layer 4 of rat barrel cortex. *J Neurophysiol* 91: 223–229, 2004.

Leiser SC, Moxon KA. Responses of trigeminal ganglion neurons during natural whisking behaviors in the awake rat. *Neuron* 53: 117–133, 2007.

Lippert MT, Takagaki K, Xu W, Huang X, Wu JY. Methods for voltage-sensitive dye imaging of rat cortical activity with high signal-to-noise ratio. *J Neurophysiol* 98: 502–512, 2007.

Luna R, Hernández A, Brody CD, Romo R. Neural codes for perceptual discrimination in primary somatosensory cortex. *Nat Neurosci* 8: 1210–1219, 2005.

Mazurek ME, Roitman JD, Ditterich J, Shadlen MN. A role for neural integrators in perceptual decision making. *Cereb Cortex* 13: 1257–1269, 2003.

Mehta SB, Whitmer D, Figueroa R, Williams BA, Kleinfeld D. Active spatial perception in the vibrissa scanning sensorimotor system. *PLoS Biol* 5: e15, 2007.

Milani H, Steiner H, Huston JP. Analysis of recovery from behavioral asymmetries induced by unilateral removal of vibrissae in the rat. *Behav Neurosci* 103: 1067–1074, 1989.

Mirabella G, Battiston S, Diamond ME. Integration of multiple-whisker inputs in rat somatosensory cortex. *Cereb Cortex* 11: 164–170, 2001.

Neimark MA, Andermann ML, Hopfield JJ, Moore CI. Vibrissa resonance as a transduction mechanism for tactile encoding. *J Neurosci* 23: 6499–6509, 2003.

O'Connor DH, Clack NG, Huber D, Komiyama T, Myers EW, Svoboda K. Vibrissa-based object localization in head-fixed mice. *J Neurosci* 30: 1947–1967, 2010a.

O'Connor DH, Peron SP, Huber D, Svoboda K. Neural activity in barrel cortex underlying vibrissa-based object localization in mice. *Neuron* 67: 1048–1061, 2010b.

Paxinos G, Watson C. *The Rat Brain in Stereotaxic Coordinates*. San Diego, CA: Academic, 2007.

Petersen CCH. The functional organization of the barrel cortex. *Neuron* 56: 339–355, 2007.

Petersen CCH, Grinvald A, Sakmann B. Spatiotemporal dynamics of sensory responses in layer 2/3 of rat barrel cortex measured in vivo by voltage-sensitive dye imaging combined with whole-cell voltage recordings and neuron reconstructions. *J Neurosci* 23: 1298–1309, 2003a.

Petersen CCH, Hahn TTG, Mehta M, Grinvald A, Sakmann B. Interaction of sensory responses with spontaneous depolarization in layer 2/3 barrel cortex. *Proc Natl Acad Sci USA* 100: 13638–13643, 2003b.

Pinto DJ, Brumberg JC, Simons DJ. Circuit dynamics and coding strategies in rodent somatosensory cortex. *J Neurophysiol* 83: 1158–1156, 2000.

Poulet JFA, Fernandez LMJ, Crochet S, Petersen CCH. Thalamic control of cortical states. *Nat Neurosci* 15: 370–372, 2012.

Ritt JT, Andermann ML, Moore CI. Embodied information processing: vibrissa mechanics and texture features shape micromotions in actively sensing rats. *Neuron* 57: 599–613, 2008.

Roitman JD, Shadlen MN. Response of neurons in the lateral intraparietal area during a combined visual discrimination reaction time task. *J Neurosci* 22: 9475–9489, 2002.

Schall JD, Thompson KG. Neural selection and control of visually guided eye movements. *Annu Rev Neurosci* 22: 241–259, 1999.

Schwarz C, Hentschke H, Butovas S, Haiss F, Stüttgen MC, Gerdjikov TV, Bergner CG, Waiblinger C. The head-fixed behaving rat—procedures and pitfalls. *Somatosens Motor Res* 27: 131–148, 2010.

Shadlen MN, Newsome WT. Neural basis of a perceptual decision in the parietal cortex (area LIP) of the rhesus monkey. *J Neurophysiol* 86: 1916–1936, 2001.

Shuler MG, Krupa DJ, Nicolelis MAL. Integration of bilateral whisker stimuli in rats: role of the whisker barrel cortices. *Cereb Cortex* 12: 86–97, 2002.

Smith PL, Ratcliff R. Psychology and neurobiology of simple decisions. *Trends Neurosci* 27: 161–168, 2004.

Sosnik R, Haidarliu S, Ahissar E. Temporal frequency of whisker movement. I. Representations in brain stem and thalamus. *J Neurophysiol* 86: 339–353, 2001.

Stüttgen MC, Rüter J, Schwarz C. Two psychophysical channels of whisker deflection in rats align with two neuronal classes of primary afferents. *J Neurosci* 26: 7933–7941, 2006.

Stüttgen MC, Schwarz C. Integration of vibrotactile signals for whisker-related perception in rats is governed by short time constants: comparison of neurometric and psychometric detection performance. *J Neurosci* 30: 2060–2069, 2010.

Stüttgen MC, Schwarz C. Psychophysical and neurometric detection performance under stimulus uncertainty. *Nat Neurosci* 11: 1091–1099, 2008.

Temereanca S, Brown EN, Simons DJ. Rapid changes in thalamic firing synchrony during repetitive whisker stimulation. *J Neurosci* 28: 11153–11164, 2008.

Towal RB, Quist BW, Gopal V, Solomon JH, Hartmann MJZ. The morphology of the rat vibrissal array: a model for quantifying spatiotemporal patterns of whisker-object contact. *PLoS Comput Biol* 7: e1001120, 2011.

Von Heimendahl M, Itskov PM, Arabzadeh E, Diamond ME. Neuronal activity in rat barrel cortex underlying texture discrimination. *PLoS Biol* 5: e305, 2007.

Wang Q, Webber RM, Stanley GB. Thalamic synchrony and the adaptive gating of information flow to cortex. *Nat Neurosci* 13: 1534–1541, 2010.

Wolfe J, Hill DN, Pahlavan S, Drew PJ, Kleinfeld D, Feldman DE. Texture coding in the rat whisker system: slip-stick versus differential resonance. *PLoS Biol* 6: e215, 2008.

Yu C, Derdikman D, Haidarliu S, Ahissar E. Parallel thalamic pathways for whisking and touch signals in the rat. *PLoS Biol* 4: e124, 2006.